On the drivers of regime shifts in the Antarctic marginal seas, exemplified by the Weddell Sea

Verena Haid[1], Ralph Timmermann[1], Özgür Gürses[1], and Hartmut H. Hellmer[1]

[1]Alfred Wegener Institute Helmholtz Centre for Polar and Marine Research, Bremerhaven, Germany

Correspondence: Verena Haid (verena.haid@awi.de)

Abstract. Recent studies found evidence for a potential future tipping point when the density of Antarctic continental shelf waters, specifically in the southern Weddell Sea, allows the onshore flow of warm waters of open ocean origin. A cold-to-warm regime shift in the adjacent ice shelf cavities entails a multiplication of ice shelf basal melt rates and can possibly trigger instabilities in the ice sheet. From a suite of numerical experiments, aimed to force such a regime shift on the continental shelf,

5 we identified the density balance between the shelf waters formed by sea ice production and the warmer water at the shelf break as the defining element for a tipping into a warm state. In our experiments, this process is reversible but with evidence for hysteresis behaviour. Using HadCM3 20th-century output as atmospheric forcing, the resulting state of the Filchner-Ronne cavity depends on the initial state. In contrast, ERA Interim forcing pushes even a warm-initialized cavity into a cold state, i.e., the system back across the reversal threshold to the cold side. However, it turns out that for forcing data perturbations of

10 a realistic magnitude, a unique and universal recipe for triggering a regime shift in Antarctic marginal seas does not exist and instead various ocean states can lead to an intrusion of off-shelf waters onto the continental shelf and into the cavities. Whether or not any given forcing or perturbation yields a density imbalance and thus allows for the inflow of warm water depends on the complex interplay between bottom topography, mean ocean state, sea ice processes, and atmospheric conditions.

1 Introduction

15 In the context of climate change, the accurate prediction of future climate evolution for different scenarios and the identification of crucial thresholds depends on a realistic representation of tipping points in the relevant climate components. For the polar environment, these components are the atmosphere, ocean, and cryosphere. A tipping point can trigger an accelerated regime shift that, without thorough knowledge of the interplay of the components involved, cannot be predicted from observations of current trends. Crossing a tipping point not only causes rapid and hard-to-predict changes after the triggering component has

20 crossed an invisible threshold, but these changes also cannot be reversed simply by a return of said triggering components to the other side of the threshold (Lenton et al., 2008; Klose et al., 2020). Typically, a reversal is either impossible or necessitates a return of the forcing components far beyond the tipping point threshold towards a 'reversal threshold'. In between these two thresholds an area of bi-stability exists, where the state of the climate depends on its own previous state (Fig. 1).

One of the possible regime shifts in polar climate is the change of the Antarctic continental shelf from a cold to a warm state.

25 Supported by atmospheric forcing, bottom topography, and/or cavity–shelf–sea interaction (Thoma et al., 2008; Nakayama
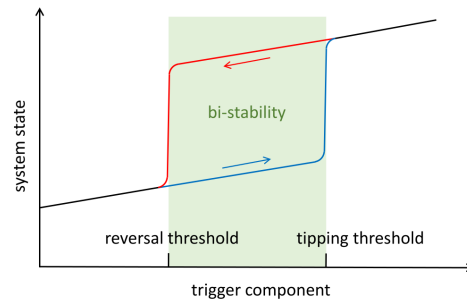
Figure 1. Schematic depiction of tipping hysteresis behaviour. The zone of bistability is shaded in green.

et al., 2013; Jourdain et al., 2017), the warming can migrate beneath fringing ice shelves (Jenkins et al., 2010) enhancing basal melting and causing instabilities of both the grounding line and the ice-shelf-feeding ice sheet (Gladstone et al., 2012; Cornford et al., 2015). For the Filchner-Ronne Ice Shelf (FRIS) in the southern Weddell Sea, such a change has been found in simulations using future climate scenarios (Hellmer et al., 2012; Naughten et al., 2021), and observations of warm water
30 intrusions on the continental shelf and into the Filchner Trough (Darelius et al., 2016; Ryan et al., 2020) seem to support the possibility of such an event in the future. Timmermann and Hellmer (2013) suggest that the decrease in sea ice production and concurrent freshening of shelf waters trigger the regime shift, which according to Hellmer et al. (2017) is irreversible as long as the meltwater input is high. In addition, Hattermann et al. (2021) emphasize the key role of off-shore winds in controlling sea ice formation, shelf water densification, and sub-ice shelf circulation.
35   Several regional models indicate further drivers of a regime shift in the southern Weddell Sea. Daae et al. (2020) identify two necessary conditions for the flow of warm water of open ocean origin into the FRIS cavity: (a) freshening of shelf waters and (b) relaxation of the Antarctic Slope Front (ASF) density gradient, which was imposed by lifting the thermocline by several hundreds of meters. Naughten et al. (2019) suggest a connection between position and intensity of the Weddell polynya and the transport of Warm Deep Water (WDW) onto the southern continental shelf caused by density changes at the shelf break. The
40 onshore flow, saltier and thus denser, enhances the sub-ice shelf circulation and melting at the FRIS base. The impact of the polynya is visible until roughly 14 years after cessation of the polynya's deep convection in their simulation. In a perturbation experiment, Bull et al. (2021) find that water mass properties of the slope current in the eastern Weddell Sea have an impact on the onshore flow of warmer waters and thus on FRIS basal melting. The recovery of the cold state after a regime shift takes 5—15 years depending on the slope current characteristics and the strength of perturbation. The findings agree with
45 earlier model results suggesting that sea ice and surface water anomalies near the Greenwich meridian have a strong impact on bottom salinity on the southern and western Weddell Sea continental shelf (Hellmer et al., 2009). In an idealized setting, Hazel and Stewart (2020) present a conceptual model in which the FRIS cavity state is determined by the water masses, either High Salinity Shelf Water (HSSW) or WDW, flooding the cavity. Plotting the cavity state against the controlling variable (meridional winds), they obtain a hysteresis with bi-stabilities as depicted in Fig. 1.

50   The EU Horizon 2020 project 'Tipping Points in Antarctic Climate Components (TiPACCs)' (www.tipaccs.eu) addresses possible near-future tipping points in the Southern Ocean and the Antarctic Ice Sheet. Within this project, we investigated the possible cold-to-warm regime shift on Antarctic continental shelves and its triggering mechanisms. In the following, we present the results of sensitivity studies with the global Finite Element Sea-ice Ocean Model (FESOM) aimed to (a) force a regime shift on the continental shelves of the Antarctic marginal seas using only manipulations of the atmospheric forcing,

55   a task proving more difficult than anticipated, but ultimately producing a range of post-shift states as well as experiments without a regime shift, and (b) identify a decisive factor that determines whether (and when) such a regime shift occurs, clearly separating experiments with a regime shift from those with a stably cold continental shelf.

    We present our model and methods used in the next chapter. In chapter 3.1, we talk about how the regime shift in the Weddell Sea does or does not occur in the different experiments, followed by an examination of the controlling mechanisms in 3.2. The

60   reversibility of the regime shift is adressed in 3.3. A discussion of our results and a summarizing chapter conclude the study.

2   Methods

2.1   Model

The Finite Element Sea ice-Ocean Model (FESOM) version 1.4 is a primitive-equation hydrostatic ocean model that is solved on a horizontally unstructured mesh (Wang et al. 2014). It contains a dynamic-thermodynamic sea ice model (Danilov et

65   al. 2015). The ice-shelf component (Timmermann et al., 2012) has been derived from the Hellmer and Olbers (1989) 3-equation model of ice shelf–ocean interaction with a velocity-dependent parameterization of boundary-layer heat and salt fluxes according to Holland and Jenkins (1999). The model has been coupled to an ice sheet model (Timmermann and Goeller, 2017), but we use it with a constant ice-shelf geometry and bottom topography derived from RTopo-2 (Schaffer et al., 2016) to reflect the present-day state as realistically as possible.

70   We use FESOM in a global configuration with a horizontal resolution ranging from 4 km in the southern Weddell and Ross Seas, and in the areas of the Antarctic coastline and ice shelves, to $\approx$120 km at the outer edge of the southern subpolar gyres and increasing to 270 km in the vast mid-latitude ocean basins (Fig. 2). The vertical discretization uses 99 unevenly spaced z-levels, starting with 5-m layers at the surface. The model has 12 layers in the uppermost 100 m and 57 layers in the uppermost 1000 m. Temperature and salinity are initialized with the World Ocean Atlas (WOA) 2013 climatography (Locarnini et al.,

75   2013; Zweng et al., 2013). The model is started from rest and spun up for 39 years using ERA Interim forcing (1979-2017; Dee et al., 2011).

2.2   Atmospheric data sets

ERA Interim: A well-established re-analyis data set of the European Centre for Medium-Range Weather Forecasts (ECMWF) (Dee et al., 2011). For the period 1979-2017, we use the 10-m zonal wind, 10-m meridional wind, 2-m air temperature, 2-m

80   dew-point temperature, evaporation, precipitation, shortwave radiation, and longwave radiation. Of these, the first four have a
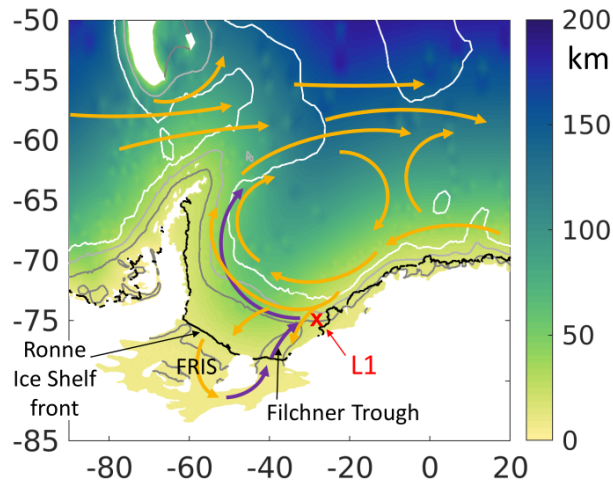
Figure 2. Detail view of the Weddell region, part of the global model domain. The grid resolution is shown in color, with ice shelf fronts (black line), 650-m isobath (dark grey), 2000-m isobath (light grey) and 3500-m isobath (white) added. Location L1 is marked with a red cross. A simplified sketch of the circulation is overlaid with orange (warm) and purple (cold) water pathways.

temporal resolution of 6 hours, the latter four of 12 hours. The data set contains 365 days per year and accounts for leap years. This data set was chosen as the basis data set for this study because Štulić et al. (2023) had tuned the model with ERA Interim forcing to match observation-based rates of sea ice formation, which play a critical role in controlling warm water intrusions into the FRIS cavity (Timmermann and Hellmer, 2013).

85   **HadCM3**: The atmospheric output of a fully coupled climate model of the Met Office Hadley Centre (Collins et al., 2011; Johns et al., 2011). The variables available to us are the 10-m zonal and meridional wind, 1.5-m air temperature and specific humidity, evaporation, precipitation, shortwave radiation, and longwave radiation. The data set contains daily fields and uses a universal, idealized year with 360 days. HadCM3 20C represents a historic simulation for the 20th century (1900-1999), HadCM3 21C-A1B covers the 21st century (2000-2099) and is based on the SRES-A1B climate scenario. This data set was 90 also used in Hellmer et al. (2012, 2017) and Timmermann and Hellmer (2013) in projection studies, where it lead to a regime shift on the Weddell Sea continental shelf. In this study, it serves as basis for a seasonal anomaly added to the ERA Interim data in some of the sensitivity experiments.

2.3   Experiments

2.3.1   Overview

95 In the framework of the TiPACCs project, we conducted an extensive suite of experiments with different perturbations of the atmospheric forcing. The choice of perturbations applied was led by roughly considering potential future trajectories of the climate state over the next century, mostly aiming for moderate rather than overly strong perturbations. A full list of experiments
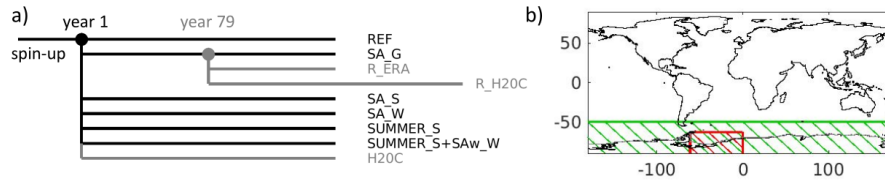
Figure 3. a) A schematic showing the branch-off points and branched-off experiments. b) The relevant regions of the different forcing applications on a map showing the global domain (_G). The circumpolar southern region (_S) is marked green, the Weddell Sea region (_W) is marked red. Please note that in our simulations ice shelf-covered areas are not affected by the atmospheric forcing.

is provided in Table S1 in the supplementary material. After 45 experiments with increasingly complicated forcing alterations that all failed to trigger a regime shift, we turned to the data set we knew from previous studies to trigger the regime shift for the Weddell Sea in sigma-coordinate models – BRIOS (Hellmer et al., 2012, 2017) and FESOM (Timmermann and Hellmer, 2013) – for inspiration and then step-by-step moved away from it again. A comparison of the HadCM3 data with ERA Interim revealed large differences in the seasonal cycle, which is why we focused on a modification of the seasonal signal in our perturbations.

We chose five perturbation experiments to be discussed here since they well cover the overall range of ocean states undergoing regime shifts (or not). The first three experiments provide useful insight on regional versus far-field influences, while the other two are closely related but land on different sides of the tipping threshold (Fig. 1) regarding the regime shift on the Weddell Sea continental shelf. Three more experiments will be analysed to investigate the reversibility of the regime shift. Details on the individual experiments follow below.

2.3.2 Reference simulation

REF: A reference/control experiment forced by unaltered ERA Interim data. The years 1979-2017 are repeated four times after a first cycle, which serves as spin-up period for this and all other experiments (see Fig. 3a). Therefore, we count the spin-up as cycle 0 and the following repeats as cycles 1 through 4.

2.3.3 Experiments addressing cause and effect of the cold-to-warm regime shift

The following five experiments are branched off from REF after the spin-up period (For more information on the effect of the forcing perturbations on the forcing variables, please refer to Table 1 and also Fig. S1 in the supplementary material.)

SA_G: The seasonal cycle of all ERA Interim variables was globally altered by adding a seasonal anomaly, also affecting the annual mean. The construction of this seasonal anomaly is described in Section 2.4 (see also Fig. S2a).

SA_S: The same alterations to the forcing data were applied as described for SA_G, but only in the region south of 50°S (Fig. 3b). North of this line the ERA Interim forcing remains unaltered.

120   **SA_W**: The same alterations to the forcing data were applied as described for SA_G, but only in the region of the Weddell Sea (south of 63°S and between 0° and 61°W; Fig. 3b). Outside of this area the ERA Interim forcing remains unaltered.

    SUMMER_S: The duration of the austral summer season is prolonged by running through every day of January three times while the austral winter months July and August are eliminated (Fig. S2b). The alteration is only applied south of 50°S (Fig. 3b). North of this line the ERA Interim forcing is unaltered.

125   **SUMMER_S+SAw_W**: Same as SUMMER_S with the exception of the zonal and meridional wind components. For the Weddell Sea region (Fig. 3b), a seasonal anomaly is added to both wind components. This seasonal anomaly is abstracted from the anomaly used in SA_W by using a fitted sine curve (with periodicity of one year; Fig. S2c) and spatial smoothing.

2.3.4   Experiments addressing reversal behaviour

Three experiments were designed to investigate reversibility of the regime shift:

130   **R_ERA**: A reversal run using unaltered ERA Interim data, same as in the reference run REF. However, the experiment starts from a post-regime-shift, warm state of the FRIS cavity (branched-off after cycle 2 of SA_G; Fig. 3a).

    R_H20C: A reversal run using unaltered HadCM3 20C data. Like R_ERA, it starts from a post-regime-shift, warm state of the FRIS cavity (branched-off after cycle 2 of SA_G; Fig. 3a).

    H20C: A run using unaltered HadCM3 20C data (same as R_H20C), but starting from a pre-regime-shift, cold state of the 135 FRIS cavity (branched-off after spin-up (cycle 0 of REF); Fig. 3a). It serves as a reference run for R_H20C.

2.4   Calculation of the seasonal anomaly for the SA_∗ experiments

The seasonal anomaly that is used in experiments SA_G, SA_S, SA_W and is the basis for the SAw_W wind field alteration was calculated by subtracting the mean seasonal cycle of ERA Interim for the period 1980-1999 from the mean seasonal cycle of HadCM3 21C-A1B for the period 2070-2089, using a 30-day running mean (see also Fig. S2a in the supplementary 140 material). This period in the second half of the 21st century was chosen because previous experiments (Timmermann and Hellmer, 2013) showed the interval to be prone to causing a regime shift on the Weddell Sea continental shelf. To make the data sets compatible, every 60th day of the HadCM3 21C-A1B data was repeated to account for the difference in length of year. In leap years, also the last day of the year is repeated.

    Additionally, the specific humidity of the HadCM3 21C-A1B data was converted to the dew point temperature before de-145 termining the mean seasonal cycle. We used both the relationship between relative humidity H_r and T_d using the Clausius-Clapeyron approximation as detailed in Stull (2017):

$$H_r := \frac{\epsilon}{\epsilon_s} \approx \frac{\epsilon_0\, e^{\frac{L}{R_v}\left(\frac{1}{T_0}-\frac{1}{T_d}\right)}}{\epsilon_0\, e^{\frac{L}{R_v}\left(\frac{1}{T_0}-\frac{1}{T_a}\right)}} \tag{1}$$

with the water vapour pressure ϵ, the saturation water vapour pressure ϵ_s, an empirical constant $\epsilon_0 = 6.113$ kPa, the latent heat L, the gas constant for pure water vapour R_v, and the reference temperature $T_0 = 273.16$ K, and the relationship between H_r 150 and H_s (Stull, 2017) combined with an approximation for ϵ_s as described by Bolton (1980), adapted for absolute temperatures:

Table 1. Regional mean values over the relevant ocean areas of the atmospheric forcing variables averaged over the 39-year forcing cycle.

area	experiment	2-m air temperature	dew point temperature	10-m zonal wind	10-m meridional wind	precipitation	evaporation	downward shortwave radiation	downward longwave radiation
		$^\circ C$	$^\circ C$	$\mathrm{m\,s^{-1}}$	$\mathrm{m\,s^{-1}}$	$10^{-8} ms^{-1}$	$10^{-8} ms^{-1}$	$\mathrm{W\,m^{-2}}$	$\mathrm{W\,m^{-2}}$
	REF	16.74	13.12	-0.274	0.068	3.732	3.969	188.3	357.8
Global	SA_G	19.32	16.73	-0.493	0.068	4.068	4.348	189.2	370.6
	SUMMER_S	16.90	13.29	-0.293	0.064	3.729	3.965	192.7	358.6
	REF	-1.13	-3.60	4.125	-0.208	2.628	1.078	109.4	273.4
South	SA_G	0.11	-0.55	4.072	-0.201	3.144	1.160	102.2	277.2
	SUMMER_S	0.13	-2.26	3.972	-0.239	2.572	1.046	143.7	279.5
	REF	-10.58	-12.89	0.548	0.857	1.234	0.167	110.7	231.3
Weddell	SA_G	-7.53	-7.37	0.427	0.529	1.842	0.311	105.6	241.8
	SUMMER_S	-7.50	-9.76	0.294	0.777	1.245	0.310	152.9	242.8

$$H_r = \frac{R_v\, p}{R_d\, \epsilon_s} H_s \approx \frac{R_v\, 6.112}{R_d} \frac{p\, H_s}{e^{\frac{17.67\,(T-T_0)}{T-29.65}}} = \frac{0.263\, p\, H_s}{e^{\frac{17.67\,(T-T_0)}{T-29.65}}} \tag{2}$$

with the gas constant for dry air R_d, and pressure p assumed to be 101.3 kPa.

The anomaly varies with location and day-of-year and is added to the ERA Interim data. Short-term and interannual vari-
155   ability of the ERA Interim data are maintained in the resulting data set, while annual mean and shape of the seasonal cycle are altered to resemble more closely those of HadCM3 21C-A1B.

3 Results

Several of our experiments using perturbations of the atmospheric forcing show a regime shift towards a sustained flow of Modified Warm Deep Water (MWDW) onto the continental shelf in the southern Weddell Sea. Of these, SA_G, SA_S, SA_W,
160   and SUMMER_S+SAw_W will be discussed in detail in the next two subsections, since they represent the range of regime shifts our experiments yielded, and the first three also allow some deductions regarding global, far-field and regional influences. SUMMER_S, on the other hand, is added to the analysis as an experiment that does not experience a regime change on the Weddell Sea continental shelf, although showing many of the characteristics that have previously been identified to accompany the regime shift.
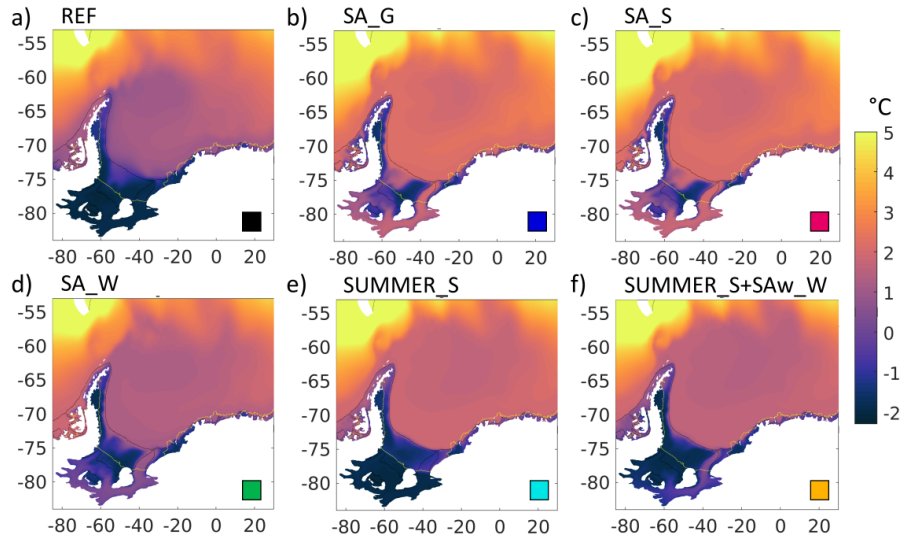
Figure 4. Temperature maximum in the water column of the Weddell Sea (mean of year 69 – 78) for experiments (a) REF, (b) SA_G, (c) SA_S, (d) SA_W, (e) SUMMER_S, and (f) SUMMER_S_SAw_W. The depicted maximum temperature of the water column is practically the same as the bottom temperature, but avoids the possibility of any 'hidden'warm water. The coloured squares in the lower right corners are intended for easier recognition of the experiments; the colors re-occur as identifiers for the different experiments in the time series plots.

165   The third subsection of this chapter examines the reversability of the regime shift. There, the experiments R_ERA and R_H20C, branched off from SA_G, are discussed and compared to their respective reference runs REF and H20C.

3.1   Warm inflow at FRIS

All presented perturbation experiments feature a warming of the Weddell Gyre (Fig. 4). Compared to 1.3 °C in REF, at 30°W core temperatures of the southern gyre branch reach 2.3 °C in SA_G and SA_S, and 1.9 °C in SUMMER_S, while SA_W (1.4
170   °C) and SUMMER_S_SAw_W (1.6 °C) experience a more moderate warming. The experiments SA_G, SA_S, SA_W, and SUMMER_S+SAw_W all feature a regime shift towards a sustained flow of Modified Warm Deep Water (MWDW) onto the continental shelf in the southern Weddell Sea with temperatures of 1.9 °C, 2.0 °C, 0.8 °C and 0.4 °C, respectively, reaching the ice shelf cavity (Fig. 4). SUMMER_S does not experience a regime shift, it is included here as a counter-example and will play an important role in Section 3.3, where we examine the decisive factors for a regime shift.
175   The experiments SA_G, SA_S, and SA_W – all applying a perturbation based on the HadCM3 21C-A1B seasonal anomaly (see Section 2.3) – clearly show a freshening and warming of the Weddell Sea continental shelf waters below 200 m (Fig. 5a,b). Between 35 and 40 years after we started to apply the perturbation, FRIS melt rates – so far on the lower end of the range based on observations (Jacobs et al., 1992; Joughin and Padman, 2003; Rignot et al., 2013) – rapidly increase up to 20 times compared to REF (Fig. 5c). During the same time interval, the Weddell Sea continental shelf appears to reach a new relatively stable state
180   with a mean temperature increased by 0.5 K in SA_W and approximately 1 K in SA_G and SA_S compared to REF. This
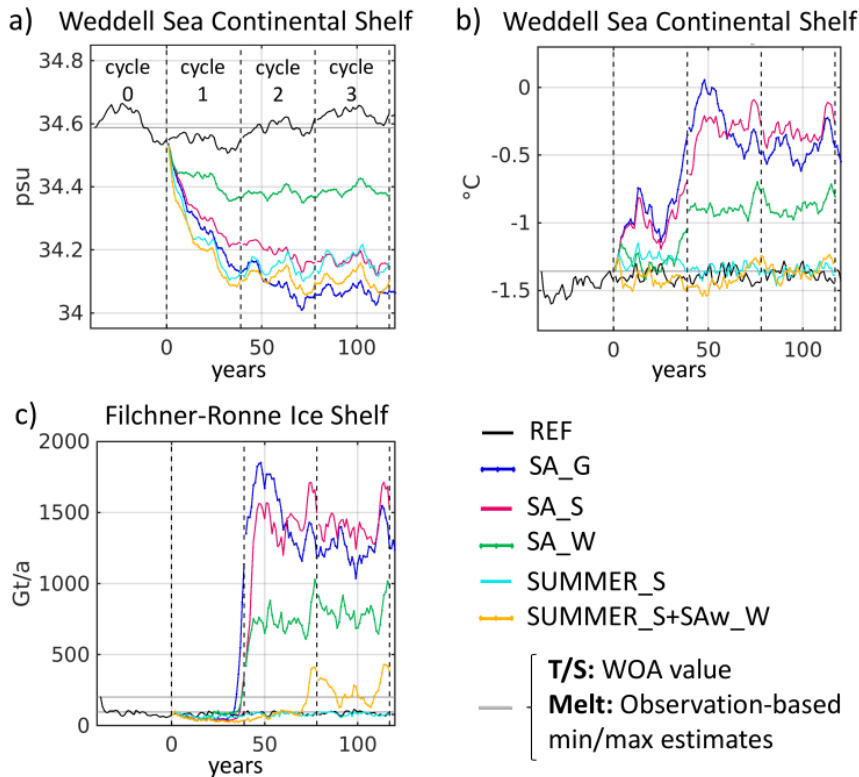
Figure 5. a) Annual mean salinity on the Weddell Sea continental shelf and, b) annual mean temperature of the Weddell Sea continental shelf (both averaged over volume 200-1000 m depth, south of 74°S, excluding the ice shelf cavity), and c) area-averaged annual mean FRIS melt rates. The observation-based estimates include studies by Jacobs et al. (1992) Joughin and Padman (2003) and Rignot et al. (2013).

temperature is dependent on the heat available in the WDW present at the continental shelf break (not the maximum in the gyre core) and temperature maps (Fig. 4) show that the temperature in the Filchner Trough has reached its maximum in all cases. Salinity is decreased by approximately 0.2 psu, 0.5 psu, and 0.4 psu, respectively, compared to REF, which after the spin-up starts with a fresh bias of 0.05 psu compared to the WOA data (Fig. 5a).

185   Once the new, warm state has been established, fluctuations in the available heat (Fig. 5b) directly impact the melt rate (Fig. 5c). We note that the strong increase in basal melt rates around year 40 is not associated with an accelerated freshening of the water on the continental shelf (compare panels a and c in Fig. 5), so that there is no evidence of a strong feedback of the enhanced meltwater supply on the water mass characteristics on the continental shelf.

Comparing the development of the continental shelf hydrography (Fig. 5a,b) between SA_G and SA_S shows that the
190   influence of forcing anomalies applied to the ocean north of the Antarctic Circumpolar Current (ACC) is comparatively small. Global forcing manipulation (SA_G) triggers a stronger reduction in shelf salinities compared to the circumpolar perturbation (SA_S), and the initial response of shelf temperatures and melt rates in SA_G surpasses that of SA_S alongside with a slightly

earlier increase in melt rates (exceeding 200 Gt/yr in year 35 vs. year 38). This initial maximum is, however, followed by a short decrease, and after year 62 both temperatures and melt rates remain below the values found in SA_S.

In SA_W, where a perturbation is applied only to the Weddell Sea, the response in both temperature and salinity is about half of what we see in SA_S, where a circumpolar perturbation is applied. The rapid melt rate increase in SA_W occurs at the same time as in SA_S, surpassing 200 Gt/yr in year 38. However, the meltrates yielded in the new steady state reflect the same factor ≈2 as found in the on-shelf temperature and salinity changes in SA_S compared to SA_W.

The differences between these three experiments clearly underline the importance of the ACC and the influence of other Antarctic regions for the Weddell Sea. The regime shift on the continental shelf is by no means an event dependent on local changes only, but is strongly influenced by far-field processes. The entire Southern Ocean is efficiently shielded from mid-latitude influence by the ACC. However, disruptions and anomalies are carried from one region of the Southern Ocean to the next by the ACC and, in the opposite direction, by the slope/coastal current with an impact on local water mass characteristics. Both air temperature and wind field exert a strong influence on the ocean. Over the ACC, the HadCM3 21C-A1B data features much higher air temperatures than ERA Interim and also the westerlies are stronger in this region (see Table 1 and Fig. S1 in the supplementary material).

The experiments SUMMER_S and SUMMER_S+SAw_W, despite showing substantial freshening on the continental shelf, do not feature a prominent increase in mean shelf water temperature (Fig. 5a,b). While in SUMMER_S, we also find no substantial rise in FRIS basal melt rates, SUMMER_S+SAw_W features a late, comparatively low increase in FRIS basal melting (≈ factor 3, Fig. 5c), triggered by a narrow inflow of (M)WDW into the Filchner Trough (Fig. 4f). These two experiments defy the expectation that a strong freshening of the continental shelf must necessarily lead to a strong warming, but also that only a strong warming on the continental shelf can provoke a multiplication of the basal melt rate at the adjacent ice shelf. The two SUMMER_* experiments will be discussed in more detail in the following subsection.

3.2 Deciding elements for warm water inflow

The experiment SUMMER_S is included in the suite of featured experiments because it demonstrates what keeps the continental shelf stable. At first glance, it seems to bring all necessary ingredients for a regime shift on the Weddell Sea continental shelf: The on-shelf water experiences thorough freshening, there is evidence of warming on the shelf in cycle 1, and both of these changes exceed what is found for SA_W, where a regime shift is triggered.

Furthermore, like SA_G and SA_S, SUMMER_S features a quick shoaling of the Antarctic Slope Front (ASF) to depths shallower than the Filchner Trough sill, while the ASF stays below sill depth almost constantly in REF and alternates around it in SA_W and SUMMER_S+SAw_W (Fig. 6). Like the other perturbation experiments, SUMMER_S also exhibits a reduction of the ACC transport (Fig. 7a) and an intensification of the Weddell Gyre circulation (Fig. 7b). The weakening of the ACC in SUMMER_S is second only to that in SUMMER_S+SAw_W and the Weddell Gyre transport (average of 39 Sv in year 30-39) is comparable to SA_G (38 Sv) and SA_S (36 Sv) and distinctively stronger than in REF (29 Sv).

The strengthening of the Weddell Gyre in SUMMER_S is also accompanied by a strong warming of WDW compared to REF (Fig. 4). Along with the much warmer southern branch of the Weddell Gyre and reduced sea ice cover goes a warm,
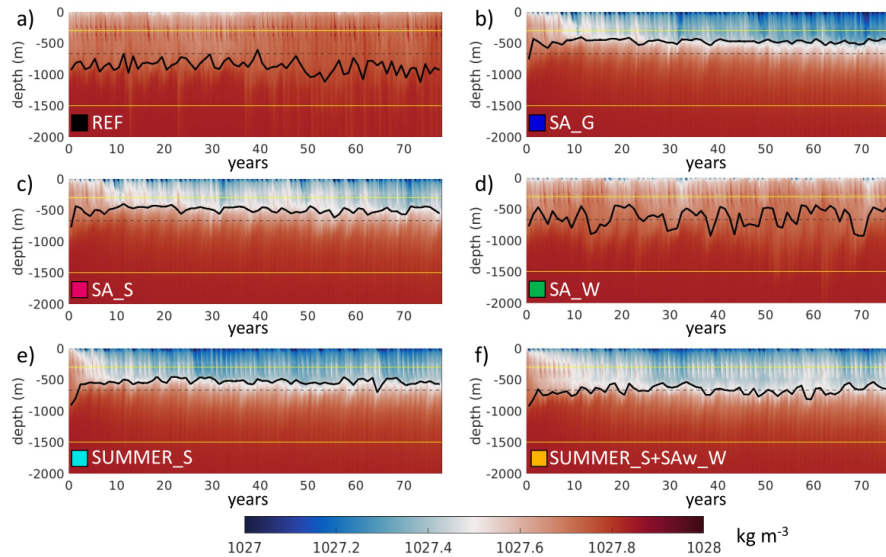
Figure 6. ASF depth (solid, black line) at continental shelf near L1 in the different experiments. The color scale shows the bottom density at the cross-section of the continental slope. ASF depth is identified by the strongest vertical temperature gradient at the bottom between the depths of 300 and 1500 m (marked with yellow lines). Additionally, the Filchner Trough sill depth is marked with a dashed black line.
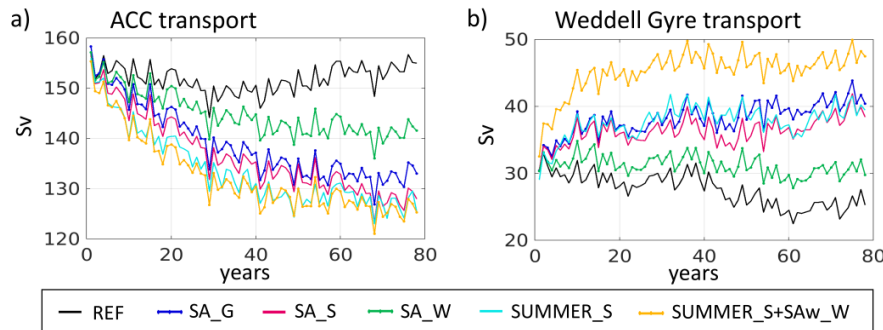
Figure 7. a) ACC transport through Drake Passage and b) transport of the southern limb of the Weddell Gyre.

surface-intensified western branch of the Weddell Gyre that follows the coastline at the tip of the Antarctic Peninsula into the Bellingshausen Sea. In all these characteristics, SUMMER_S is no different from experiments featuring regime shifts (e.g. SA_G and SA_S), but the continental shelf and the ice shelf cavity in SUMMER_S remain protected from the off-shelf

230 changes.

The crucial criterion for the warm water to cross the continental shelf and fill the ice shelf cavity turns out to be the balance between the density off-shelf at sill depth and the density of the densest water produced by sea ice formation on the continental shelf. In the Weddell Sea, the most active polynya exists in front of Ronne Ice Shelf (Haid and Timmermann, 2013) with a
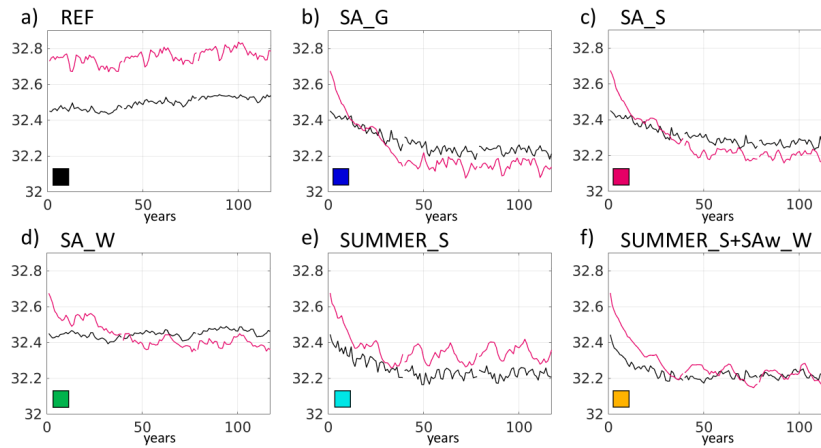
Figure 8. Annual mean values of maximum density σ_1 (potential density anomaly with reference pressure of 1000 dbar; reference density 1000 kg m^{-3}) along the Ronne Ice Shelf front (red) and bottom density (σ_1) at 670 m depth at the continental shelf break at location L1 marked in Fig. 2 (black) for experiments (a) REF, (b) SA_G, (c) SA_S, (d) SA_W, (e) SUMMER_S, and (f) SUMMER_S_SAw_W. The depth of L1 is determined by the z-level closest to the Filchner Trough sill depth, which in the model is 640 m, slightly lower than in reality.

seasonal fluctuation of the location of the densest water that is either found on the eastern or the western side of the Ronne Ice

235 Shelf front. We therefore compare the maximum bottom density found along the Ronne Ice Shelf front as a measure of HSSW properties with the bottom density at the shelf break at a position east of (i.e. upstream from) the Filchner Trough sill at 670 m depth (approximate sill depth, location L1 in Fig. 2) as a measure for the properties of the WDW at issue. As seen in Fig 8a, REF densities for the HSSW in front of Ronne Ice Shelf are typically 0.3 kg m^{-3} higher than for the WDW at the shelf break, with a slight positive trend in both time series.

240   In the perturbation experiments SA_G and SA_S (Fig. 8b, c), the HSSW features a strong density loss in the first 4-5 decades as a reaction to the altered atmospheric forcing. Although also WDW density decreases in these experiments (by between 0.2 and 0.22 kg m^{-3}), at around year 30 it becomes the denser of the two water masses. A direct comparison between these two experiments shows that the WDW density loss is slightly diminished and slowed down by applying the forcing perturbation only to the southern part of the globe. With further restriction of the perturbation area in SA_W (Fig. 8d), the off-shelf density

245 remains relatively stable. It exhibits a slight positive trend, but smaller than in REF.

    For experiments SA_G, SA_S and SA_W, the maximum density found on the continental shelf off Ronne Ice Shelf decreases by 0.3-0.6 kg m^{-3} (red lines in Fig. 8 b-d), since sea ice formation is strongly reduced by our perturbation of the atmospheric forcing. While SA_G is the experiment with the strongest off-shelf density loss, its on-shelf density decreases even more. Thus, in all cases, the on-shelf density decreases below the off-shelf density after between 30 and 40 years, allowing the warm

250 off-shelf waters to replace the cold waters in the FRIS cavity.

In SUMMER_S (Fig 8e), the off-shelf density remains below the on-shelf density and although water mass characteristics have changed on-shelf and off-shelf, the continental shelf remains protected by a persisting, albeit more vulnerable density contrast. It then only takes a change in the regional wind pattern (SUMMER_S+SAw_W) to further inhibit sea ice production and reduce the on-shelf density. The weaker northward winds in HadCM3 21C-A1B (see Table 1 and Fig. S1k) cause a more persistent sea ice cover in the southwestern Weddell Sea, and therefore a decrease of both on-shelf salinity (Fig 5a) and the maximum density in front of Ronne Ice Shelf (Fig 8f). In contrast to SUMMER_S, the SUMMER_S+SAw_W on-shelf density dips, at least temporarily, below the off-shelf density, immediately triggering warm water flow onto the continental shelf and into the cavity via the Filchner Trough.

After year 70 in SUMMER_S+SAw_W, the maxima and minima seen in the FRIS basal mass loss (Fig. 5c) can be clearly associated with the extremes in the maximum density in front of Ronne Ice Shelf (Fig. 8f). In this case, the density balance is so sensitive that the mean basal melting of FRIS is controlled by sea ice production on the continental shelf. One should note, however, that salinity – the governing control on density in the region – is a product not only of local processes but of the accumulated history of the water parcel (Haid et al., 2015). In the other experiments, once a warm state is established (year 40+), mean FRIS basal melting shows a clear dependence on the mean temperature on the continental shelf (cf Fig. 5b and c).

3.3 Reversibility and evidence of hysteresis behaviour

In order to fulfill the strict definition of a tipping point, the return from a tipped, warm ocean to the initial, cold state should not be as easy as just reversing forcing conditions back over the tipping threshold. Instead, an additional effort to push the system beyond a reversal threshold should be required. For a tipping point, we expect hysteresis behaviour when switching from one state to the other compared to the reverse (see also Fig. 1).

As a quick test for evidence of the regime shift on continental shelf actually being a tipping point, we branched off two reversal experiments, R_ERA and R_H20C after cycle 2 of SA_G (see Fig. 5). These experiments thus start with a warm Weddell Sea continental shelf and show its evolution for current/last century atmospheric conditions.

The results show that an instantaneous return to unaltered ERA Interim forcing (R_ERA) causes a rapid decrease of FRIS basal melt rates (purple line in Fig. 9a), which is linked to a rapid cooling (Fig. 9b) and salinity increase (Fig. 9c) on the continental shelf. As soon as the shelf waters off Ronne Ice Shelf (Fig. 9e) are denser than the waters off-shore at sill depth (Fig. 9d), they inevitably intrude into the cavity due to the southward sloping bathymetry. Depending on the volume of dense water produced by sea ice formation, this will diminish or prevent the flow of warm water into the cavity.

Within two decades, a thermal state similar to the REF cold state is re-established on the southern Weddell Sea continental shelf (Fig. 9a,b). Basal melt rates and shelf temperatures return to pre-tipping levels even though shelf salinity is still slightly fresher and it takes a few decades to return to its cold-state values (Fig. 9c). Again, the decisive factor is the density balance between the waters influenced by sea ice production on the continental shelf and the off-shelf waters of the Weddell Gyre. The fast increase of the on-shelf water density (Fig. 9d) stops the inflow of WDW/MWDW into the cavity, which gets replaced in time by cold HSSW.
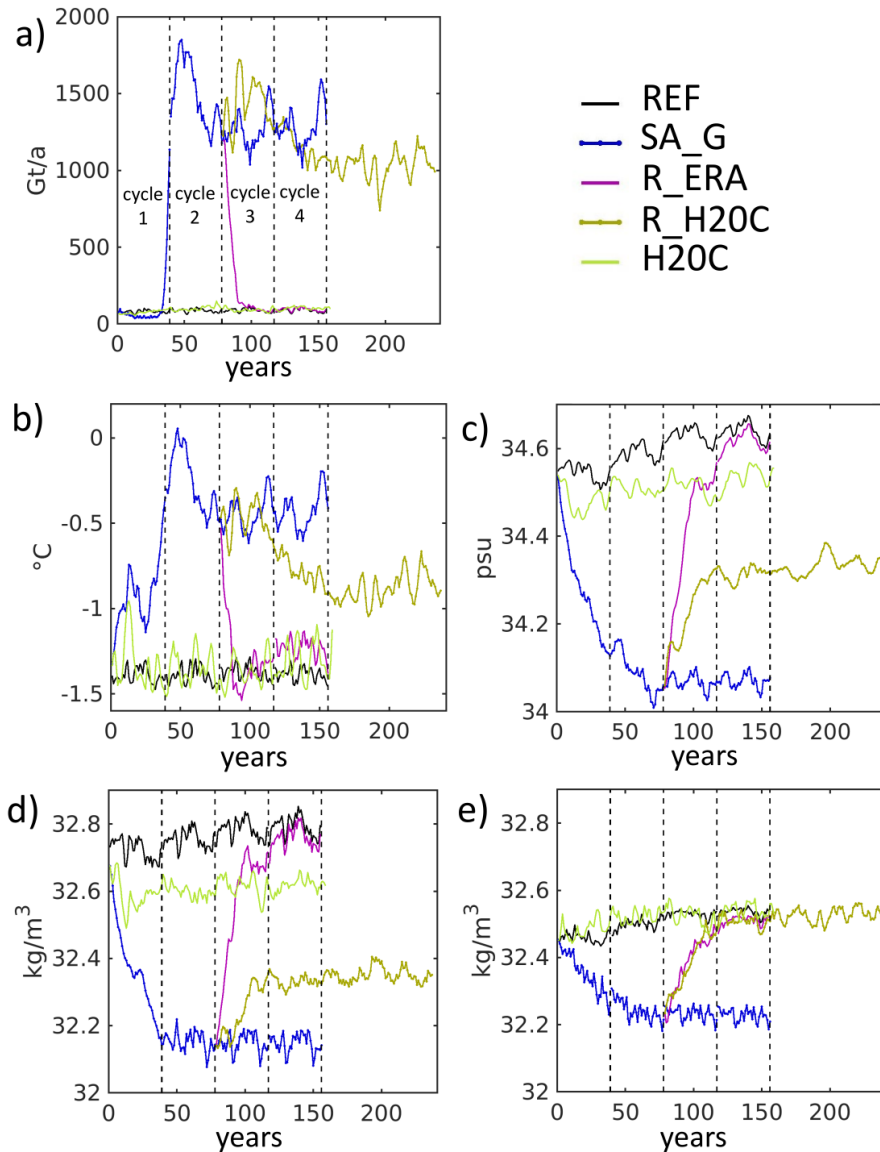
Figure 9. Area-averaged annual mean values of (a) FRIS basal mass loss, (b) temperature and (c) salinity on the Weddell Sea continental shelf (both below a depth of 200 m and south of 74°S), (d) maximum density at the Ronne Ice Shelf front, and (e) bottom density near the Filchner Trough sill (Location L1) for the experiments listed in the upper right corner.

Using the 20th-century HadCM3 data to force the model starting from a warm state (R_H20C) leads to a gradual reduction of the melt rates (Fig. 9a). The inflow of warm water does not stop, since the density of the shelf water remains below the off-shelf water density. The existing density difference even facilitates a stronger inflow during the next 3 decades. In the long

term, however, basal melt rates decrease because of a cooling of WDW/MWDW by 2 K from 1.1 °C in SA_G (averaged over years 69-78) to -1.0 °C in R_H20C (years 108-117) at location L1 (Fig. 2).

Starting from a cold state and using the same unaltered forcing (20th-century HadCM3 data, experiment H20C), the model stays in a cold state (Fig. 9). The forcing yields a higher long-term mean for the on-shelf temperatures and generally lower salinities than REF. Although the density difference is reduced compared to REF and it features a higher interannual variability, the continental shelf remains stably in a cold state.

4   Discussion

We identified a density balance as the decisive and defining factor for a regime shift on the southern Weddell Sea continental shelf. Neither the evolution of the on-shelf salinity, of the ASF height, nor of the ACC or Weddell Gyre transports alone allowed to differentiate between a stable experiment (SUMMER_S) and a group of experiments undergoing a regime shift (SA_G, SA_S, SA_W, and SUMMER_S+SAw_W). Only the density difference between WDW and dense shelf water reliably allows this differentiation.

In order to penetrate onto the continental shelf and into the ice shelf cavities, the water at the shelf break at sill depth has to literally outweigh the water produced by sea ice formation on the continental shelf (with some inaccuracies due to mixing processes). In a situation with moderate density gradients, this may lead to a protracted period of temporary and especially seasonal onshore flow of WDW, but any process causing the circumpolar waters to freshen less than the shelf waters will eventually tip the density balance in favour of the waters of open-ocean origin. In consequence, the warmer off-shelf waters will replace the cold shelf waters in the cavity and enhance basal melting. We suppose that this continental shelf/shelf break process does exist not only in the Weddell Sea but in all other Antarctic marginal seas unless strong local influences (e.g., winds, bottom topography) create an additional barrier at the continental shelf break or on the continental shelf.

In our experiments, e.g., the Ross Sea remains stable (see also Fig. S3-S5 in the supplementary material), while in the Prydz Bay CDW gains access into the Amery Ice Shelf cavity even faster than for the regime shift in the Weddell Sea in SA_G, SA_S, SUMMER_S and SUMMER_S+SAw_W (Fig. S3 & S4), and the density time series (Fig. S6) confirm our findings obtained for the Weddell Sea. Our model geometry for the Prydz Bay is subject to large uncertainties, which is why the region serves only as a proof of concept for the density balance and is not presented in the main article.

It is no surprise that water density is crucial for a regime shift that allows WDW to penetrate onto the continental shelf and into fringing ice shelf cavities. Daae et al. (2020) found that a shoaling of the thermocline is important in triggering a warm inflow. In their regional model study, this was achieved by an artificial manipulation of the boundary conditions that also entailed a lifting of the halocline and thus an increase in off-shelf water density at sill depth.

However, an increase of salinity at these depths is not a trend we observe around Antarctica (Schmidtko et al., 2014) or expect for the future. Instead, increased ice melt – including sea ice, ice shelves, and icebergs – all around Antarctica causes a freshening of the Southern Ocean, especially in the coastal and slope currents (Strass et al., 2020). In accordance with these expectations for the future, we see freshening on- and off-shelf in all our experiments that apply at least a circumpolar

320 perturbation. The waters generally become warmer and fresher and therefore lighter. Only, if the on-shelf density falls below the density of the off-shelf waters at sill depth, the latter will enter the continental shelf and fill up the deep parts of the ice shelf cavities. Our findings are also in accordance with the conceptual model proposed by Hazel and Stewart (2020), where the water mass density determines whether HSSW or WDW floods the ice shelf cavity, but include the evolution of the WDW density.

325 The Weddell Sea continental shelf has a unique bathymetry which contributes to the vulnerability of its fringing ice shelves. The Filchner Trough with a sill depth of approximately 600 m allows deeper and denser off-shelf waters an easy access path. However, on-shelf salinity is a crucial factor when comparing the vulnerabilities of the Weddell and Ross Seas. During the spin-up cycle, our model experiences a slight freshening of the Weddell Sea and a salinity increase of the Ross Sea continental shelf. While the latter does indeed feature more saline water than the former, this difference is likely exaggerated in our model,

330 as evidenced by the bias in reference to the WOA data used for initialisation (see also Fig. S4a in the supplementary material). Since the salinity dominates density on the continental shelves around Antarctica, this creates a much higher density threshold for the Ross Sea and keeps its continental shelf cold in all our experiments. A study by Comeau et al. (2022), where a fresh bias on the Weddell Sea shelf led to an unwanted regime shift, supplies further evidence for the adverse effects of salinity biases in models in this context.

335 With our model set-up, even for FRIS, it turns out difficult to yield a regime change in the cavity by simple or idealized perturbations of the atmospheric forcing. As mentioned in Section 2.3, in the framework of the TiPACCs project we conducted more than 70 experiments with different alterations of the atmospheric forcing. Of these, only a minority resulted in a change of the Weddell Sea to a warm-shelf state. This lack of an 'easy recipe' within reasonable bounds reminds us that climate is a complex system with omnipresent non-linearities.

340 In our 'successful' experiments, however, the response was quicker than what Naughten et al. (2021) obtained for an abrupt change in atmospheric forcing, and with smaller changes, particularly in air temperature. The atmospheric forcing used in all our experiments experiencing a regime shift has some relationship to the HadCM3 21C-A1B output and involves changes in all or all-but-one forcing variables. All manipulations of a single or up-to-three atmospheric variables failed in inducing sustained warm water flow onto the continental shelf. Although air temperature and wind components were found to be important in the

345 process, a manipulation of only these three variables in the same way as in SA_G was not sufficient to trigger the inflow.

After the regime shift to a warm state on the continental shelf, Hellmer et al. (2017) claim that the increased amount of melt water leads to a positive feedback on the cavity overturning circulation supporting a sustained inflow and an enhancement of basal melt rates. Therefore, a resistance of the system against a reversal is expected. However, the hysteresis behaviour, which is required for the strict definition of a tipping point, is not easy to demonstrate for a regime shift in an Antarctic ice shelf

350 cavity. While Hazel and Stewart (2020) suceeded in mapping out a clear hysteresis curve for FRIS depending on meridional wind modifications (using a regional set-up and thus neglecting far-field influences on the Weddell Gyre), Caillet et al. (2022) could not find evidence of hysteresis investigating a possible past regime shift on the Amundsen Sea continental shelf. Although the evolution of the water mass characteristics on the continental shelf in our experiments provides no direct evidence toward the effect of a meltwater feedback (Fig. 5), our experiments clearly show evidence of hysteresis behaviour: Depending on the

starting state of the continental shelf, two different shelf states are reached for the same forcing data set (HadCM3 20C). In contrast, using ERA Interim data drives the system back from warm to cold very quickly, indicating that the meltwater feedback alone is not sufficient to maintain the warm regime as a new stable state. Based on our findings, we would locate the HadCM3 data for the 20th century, used in runs H20C and R_H20C, in the zone of bi-stability in the simplified scheme of Fig. 1, while placing the ERA Interim forcing to the left of the reversal threshold (both initial states yield the same, cold final state). The forcing used for SA_G is located to the right of the tipping threshold (see also Fig. S7 in the supplementary material).

Our findings also underline that the range of bi-stability may not be very large and that with our still limited understanding of the complex system, it can be difficult to find an atmospheric forcing data set that actually falls into this range. It may well be that current and/or last-century atmospheric conditions fall on the left side of the reversal threshold. Some caution is also advised: The climate system and its regional subsystems follow a complex interplay of a multitude of variables, which makes the 2D schematic a strong simplification of a multi-dimensional problem.

Model studies with FESOM coupled to an ice sheet/ice shelf model (Timmermann and Goeller, 2017) show that enhanced basal melting of FRIS leads to an accelerated ice flow across the grounding line and thus contributes to global sea level rise. The model also demonstrates that the feedback of changing ice shelf geometry on cavity circulation does not cause qualitative differences in the relevant processes of ocean – ice shelf interaction. Compared to uncoupled simulations with constant present-day cavity geometry, the coupled simulations yield a slightly stronger increase of basal melt rates in case of the ocean tipping into a warm state, but again results are not qualitatively different. We can therefore be confident that our results faithfully reflect the essential feedbacks between the different components of our model climate system.

By design, our study can only address regime shifts in the ocean (in the open ocean just as much as in sub-ice cavities); it cannot assess tipping points or instabilities in the ice sheet (e.g. accelerated ice mass flux through the speed-up of ice streams) or coupled oceanic-cryospheric tipping points, like a marine ice sheet instability with irreversible grounding line retreat. In the framework of the TiPACCs project, several studies on ice shelf tipping points have already been conducted (Reese et al., 2022; Urruty et al., 2022) and coupled model studies are on the way.

5 Conclusions

In our modelling study on the change of the ocean state on the Weddell Sea continental shelf, we identify the density balance between the off-shelf water at sill depth and the water produced by sea ice formation on the continental shelf as the decisive factor determining whether the flow of off-shelf water into the deepest part of the continental shelf and the ice shelf cavities below sill depth is possible. Our experiments confirm the possibility for such a regime shift within the next 100 years for the FRIS cavity but not for the Ross Ice Shelf cavity. While the sill depth of the continental shelf certainly is one of the influential differences between the two regions, the higher on-shelf salinity in the Ross Sea in our simulations is more relevant in the context of a cold-to-warm regime shift. In model studies, salinity biases on the Antarctic continental shelf – positive or negative – strongly influence the simulated vulnerability of the shelf to warm water intrusions. In our model, it leads to a larger

density difference between the on-shelf waters and the warm Circumpolar Deep Water and keeps the Ross Sea density balance stable in all our experiments.

We find that the ice shelf cavities may be better protected from the intrusion of warm WDW/CDW than previously expected (e.g., Hellmer et al., 2012). In a realistic future scenario not only the dense shelf waters linked to sea ice formation will undergo changes, but also the ACC and CDW/WDW characteristics, and the entire Southern Ocean will be affected by these changes. Both HSSW and WDW are expected to lose density but at different rates, since HSSW is primarily influenced by local atmospheric events while the WDW/CDW characteristics depend more on the far-field. It is noteworthy, however, that a universal recipe for a regime shift in the Antarctic marginal seas does not exist, but that such a shift can occur under diverse circumstances and depends on local influences ranging from bottom topography to atmospheric conditions.

Our results support the assumption that a cold-to-warm regime shift on the Weddell Sea continental shelf is a tipping point with hysteresis behaviour. The zone of bi-stability between the thresholds of tipping and reversal, however, may not be very wide. Potentially, present-day atmospheric conditions are on the 'cold' side of the bi-stability zone of the hysteresis.

Data availability. The data contained in the Figures as well as the ocean state in the Weddell region for all featured experiments are publicly available under doi:10.5281/zenodo.8086825 (Part I) and doi:10.5281/zenodo.8086878 (Part II).

Author contributions. VH conducted the numeric experiments, analysed and visualised the results and led the writing process; OG provided the model geometry, read and commented on the manuscript; HHH conceived the idea for the study; RT and HHH contributed to the interpretation of results and to writing the manuscript.

Competing interests. None of the authors have any competing interests.

Acknowledgements. This work is part of the TiPACCs project, which receives funding from the European Union's Horizon 2020 research and innovation programme under grant agreement no. 820575. RT is supported by the Helmholtz Climate Initiative REKLIM (Regional Climate Change), a joint research project of the Helmholtz Association of German research centres (HGF). The work relied heavily on computational resources provided by the North German Supercomputing Alliance (HLRN). We thank our reviewers and our editor for their work and their helpful comments on the manuscript.

References

Bolton, D.: The Computation of Equivalent Potential Temperature, Monthly Weather Review, 108, 1046 – 1053, https://doi.org/10.1175/1520-0493(1980)108<1046:TCOEPT>2.0.CO;2, 1980.

Bull, C. Y. S., Jenkins, A., Jourdain, N. C., Vankova, I., Holland, P. R., Mathiot, P., Hausmann, U., and Sallee, J.-B.: Remote control of Filchner-Ronne Ice Shelf melt rates by the Antarctic Slope Current, J. Geophys. Res., 126, https://doi.org/10.1029/2020JC016550, 2021.

Caillet, J., Jourdain, N. C., Mathiot, P., Hellmer, H. H., and Mouginot, J.: Drivers and reversibility of abrupt ocean state transitions in the Amundsen Sea, Antarctica, Earth and Space Science Open Archive, p. 23, https://doi.org/10.1002/essoar.10511518.1, 2022.

Collins, M., Booth, B. B. B., Bhaskaran, B., Harris, G. R., Murphy, J. M., Sexton, D. M. H., and Webb, M. J.: Climate model errors, feedbacks and forcings: a comparison of perturbed physics and multi-model ensembles, Climate Dynamics, 36, 1737–1766, https://doi.org/10.1007/s00382-010-0808-0, 2011.

Comeau, D., Asay-Davis, X. S., Begeman, C. B., Hoffman, M. J., Lin, W., Petersen, M. R., Price, S. F., Roberts, A. F., Van Roekel, L. P., Veneziani, M., Wolfe, J. D., Fyke, J. G., Ringler, T. D., and Turner, A. K.: The DOE E3SM v1.2 Cryosphere Configuration: Description and Simulated Antarctic Ice-Shelf Basal Melting, Journal of Advances in Modeling Earth Systems, 14, e2021MS002 468, https://doi.org/https://doi.org/10.1029/2021MS002468, 2022.

Cornford, S. L., Martin, D. F., Payne, A. J., Ng, E. G., Le Brocq, A. M., Gladstone, R. M., Edwards, T. L., Shannon, S. R., Agosta, C., van den Broeke, M. R., Hellmer, H. H., Krinner, G., Ligtenberg, S. R. M., Timmermann, R., and Vaughan, D. G.: Century-scale simulations of the response of the West Antarctic Ice Sheet to a warming climate, The Croysphere, 9, 1579–1600, https://doi.org/10.5194/tc-9-1579-2015, 2015.

Daae, K., Hattermann, T., Darelius, E., Mueller, R. D., Naughten, K. A., Timmermann, R., and Hellmer, H. H.: Necessary conditions for warm inflow toward the Filchner Ice Shelf, Weddell Sea, Geophys. Res. Letters, 47, https://doi.org/10.1029/2020GL089237, 2020.

Darelius, E., Fer, I., and Nicholls, K. W.: Observed vulnerability of Filchner-Ronne Ice Shelf to wind-driven inflow of warm deep water, Nature Comm., 7:12300, https://doi.org/10.1038/ncomms12300, 2016.

Dee, D. P., Uppala, S. M., Simmons, A. J., Berrisford, P., Poli, P., Kobayashi, S., Andrae, U., Balmaseda, M. A., Balsamo, G., Bauer, P., Bechtold, P., Beljaars, A. C. M., van de Berg, L., Bidlot, J., Bormann, N., Delsol, C., Dragani, R., Fuentes, M., Geer, A. J., Haimberger, L., Healy, S. B., Hersbach., H, H. E. V., Isaksen, L., Kållberg, P., Köhler, M., Matricardi, M., McNally, A. P., Monge-Sanz, B. M., Morcrette, J.-J., Park, B.-K., Peubey, C., de Rosnay, P., Tavolato, C., Thépaut, J.-J., and Vitar, t. F.: The ERA-interim reanalysis: Configuration and performance of the data assimilation system, Q. J. R. Meteorol. Soc., 137, 553–597, https://doi.org/10.1002/qj.828, 2011.

Gladstone, R. M., Lee, V., Rougier, J., Payne, A. J., Hellmer, H. H., Le Brocq, A., Shepherd, A., Edwards, T. L., Gregory, J., and Cornford, S. L.: Calibrated prediction of Pine Island Glacier retreat during the 21st and 22nd centuries with a coupled flowline model, Earth Planet. Sci. Lett., 333–334, 191–199, https://doi.org/10.1016/j.epsl.2012.04.022, 2012.

Haid, V. and Timmermann, R.: Simulated heat flux and sea ice production at coastal polynyas in the southwestern Weddell Sea, J. Geophys. Res., 118, 2640–2652, https://doi.org/10.1002/jgrc.20133, 2013.

Haid, V., Timmermann, R., Ebner, L., and Heinemann, G.: Atmospheric forcing of coastal polynyas in the south-western Weddell Sea, Antarctic Science, 27, 388–402, https://doi.org/10.1017/S0954102014000893, 2015.

Hattermann, T., Nicholls, K. W., Hellmer, H. H., Davis, P. E. D., Janout, M. A., Østerhus, S., Schlosser, E., Rohardt, G., and Kanzow, T.: Observed interannual changes beneath Filchner-Ronne Ice Shelf linked to large-scale atmospheric circulation, Nature Comm., 12, https://doi.org/10.1038/s41467-021-23131-x, 2021.

Hazel, J. E. and Stewart, A. L.: Bistability of the Filchner-Ronne Ice Shelf cavity circulation and basal melt, J. Geophys. Res., 124, e2019JC015 848, https://doi.org/10.1029/2019JC015848, 2020.

Hellmer, H. H. and Olbers, D. J.: A two-dimensional model for the thermohaline circulation under an ice shelf, Antarctic Science, 1, 325–336,
450   1989.

Hellmer, H. H., Kauker, F., and Timmermann, R.: Weddell Sea anomalies: Excitation, propagation, and possible consequencs, Geophys. Res. Letters, 36, L12 605, https://doi.org/10.1029/2009GL038407, 2009.

Hellmer, H. H., Kauker, F., Timmermann, R., Determann, J., and Rae, J.: Twenty-first-century warming of a large Antarctic ice-shelf cavity by a redirected coastal current, Nature, 485, 225–228, https://doi.org/10.1038/nature11064, 2012.

455 Hellmer, H. H., Kauker, F., Timmermann, R., and Hattermann, T.: The fate of the southern Weddell Sea continental shelf in a warming climate, jc, 30, 4337–4350, https://doi.org/10.1175/JCLI-D-16-0420.1, 2017.

Holland, D. M. and Jenkins, A.: Modeling thermodynamic ice-ocean interactions at the base of an ice shelf, J. Phys. Oceanogr., 29, 1787–1800, 1999.

Jacobs, S. S., Hellmer, H. H., Doake, C. S. M., Jenkins, A., and Frolich, R. M.: Melting of ice shelves and the mass balance of Antarctica, J.
460   Glaciol., 38, 375–387, 1992.

Jenkins, A., Dutrieux, P., Jacobs, S., McPhail, S., Perrett, J., Webb, A., and White, D.: Observations beneath Pine Island Glacier in West Antarctica and implications for its retreat, Nature Geoscience, 3, 468–472, https://doi.org/10.1038/ngeo890, 2010.

Johns, T. C., Royer, J.-F., Höschel, I., Huebener, H., Roeckner, E., Manzini, E., May, W., Dufresne, J.-L., Otterå, O. H., Vuuren, D. P., Salas y Melia, D., Giorgetta, M. A., Denvil, S., Yang, S., Fogli, P. G., Körper, J., Tjiputra, J. F., Stehfest, E., and Hewitt, C. D.: Climate change
465   under aggressive mitigation: The ENSEMBLES multi-model experiment, Climate Dyn., 37, 1975–2003, https://doi.org/10.1007/s00382-011-1005-5, 2011.

Joughin, I. and Padman, L.: Melting and freezing beneath Filchner-Ronne Ice Shelf, Antarctica, Geophys. Res. Letters, 30, 1477, 2003.

Jourdain, N. C., Mathiot, P., Merino, N., Durand, G., Le Sommer, J., Spence, P., Dutrieux, P., and Madec, G.: Ocean circulation and sea-ice thinning induced by melting ice shelves in the Amundsen Sea, J. Geophys. Res., 122, 2550–2573, https://doi.org/10.1029/2003GL016941,
470   2017.

Klose, A. K., Karle, V., Winkelmann, R., and Donges, J. F.: Emergence of cascading dynamics in interacting tipping elements of ecology and climate, R. Soc. Open Sci., 7:200599, https://doi.org/10.1098/rsos.200599, 2020.

Lenton, T. M., Held, H., E., K., Hall, J. W., Lucht, W., Rahmstorf, S., and Schellnhuber, H. J.: Tipping elements in the Earth's climate system, Proc. Natl Acad. Sci. USA, 105, 1786–1793, https://doi.org/10.1073/pnas.0705414105, 2008.

475 Locarnini, R. A., Mishonov, A. V., Antonov, J. I., Boyer, T. P., Garcia, H. E., Baranova, O. K., Zweng, M. M., Paver, C. R., Reagan, J. R., Johnson, D. R., Hamilton, M., and Seidov, D.: World Ocean Atlas 2013, Volume 1: Temperature, in: NOAA Atlas NESDIS 73, edited by Levitus, S. and Mishonov, A., p. 40 pp, 2013.

Nakayama, Y., Schröder, M., and Hellmer, H. H.: From circumpolar deep water to the glacial meltwater plume on the eastern Amundsen Shelf, Deep-Sea Res., 77, 50–62, https://doi.org/10.1016/j.dsr.2013.04.001, 2013.

480 Naughten, K. A., Jenkins, A., Holland, P. R., Mugford, R. I., Nicholls, K. W., and Munday, D. R.: Modeling the Influence of the Weddell Polynya on the Filchner–Ronne Ice Shelf Cavity, J. Climate, 32, 5289–5303, https://doi.org/10.1175/JCLI-D-19-0203.1, 2019.

Naughten, K. A., De Rydt, J., Rosier, S. H. R., Jenkins, A., Holland, P. R., and Ridley, J. K.: Two-timescale response of a large Antarctic ice shelf to climate change, Nature Comm., 12:1991, https://doi.org/10.1038/s41467-021-22259-0, 2021.

Reese, R., Garbe, J., Hill, E. A., Urruty, B., Naughten, K. A., Gagliardini, O., Durand, G., Gillet-Chaulet, F., Chandler, D., Langebroek, P. M., and Winkelmann, R.: The stability of present-day Antarctic grounding lines – Part B: Possible commitment of regional collapse under current climate, The Cryosphere Discussions, 2022, 1–33, https://doi.org/10.5194/tc-2022-105, 2022.

Rignot, E., Jacobs, S. S., Mouginot, J., and Scheuchl, B.: Ice shelf melting around Antarctica, Science, 341, 266–270, https://doi.org/10.1126/science.1235798, 2013.

Ryan, S., Hellmer, H. H., Janout, M., Darelius, E., Vignes, L., and Schröder, M.: Exceptionally warm and prolonged flow of Warm Deep Water toward the Filchner-Ronne Ice Shelf in 2017, Geophys. Res. Letters, 47, e2020GL088 119, https://doi.org/10.1029/2020GL088119, 2020.

Schaffer, J., Timmermann, R., Arndt, J. E., Kristensen, S. S., Mayer, C., Morlighem, M., and Steinhage, D.: A global, high-resolution data set of ice sheet topography, cavity geometry, and ocean bathymetry, Earth System Science Data, 8, 543–557, https://doi.org/10.5194/essd-8-543-2016, 2016.

Schmidtko, S., Heywood, K. J., Thompson, A. F., and Aoki, S.: Multidecadal warming of Antarctic waters, Science, 346, 1227–1231, https://doi.org/10.1126/science.1256117, 2014.

Strass, V. H., Rohardt, G., Kanzow, T., Hoppema, M., and Boebel, O.: Multidecadal Warming and Density Loss in the Deep Weddell Sea, Antarctica, Journal of Climate, 33, 9863 – 9881, https://doi.org/10.1175/JCLI-D-20-0271.1, 2020.

Stull, R.: Practical Meteorology: An Algebra-based Survey of Atmospheric Science - version 1.02b, 2017.

Thoma, M., Jenkins, A., Holland, D., and Jacobs, S. S.: Modelling Circumpolar Deep Water intrusions on the Amundsen Sea continental shelf, Antarctica, Geophys. Res. Letters, 35, 2008.

Timmermann, R. and Goeller, S.: Response to Filchner-Ronne Ice Shelf cavity warming in a coupled ocean-ice sheet model - Part 1: The ocean perspective, Ocean Science, 13, 765–776, https://doi.org/10.5194/os-13-765-2017, 2017.

Timmermann, R. and Hellmer, H. H.: Southern Ocean warming and increased ice shelf basal melting in the twenty-first and twenty-second centuries based on coupled ice-ocean finite-element modelling, Ocean Dyn., 63, 1011–1026, https://doi.org/10.1007/s10236-013-0642-0, 2013.

Timmermann, R., Wang, Q., and Hellmer, H. H.: Ice shelf basal melting in a global finite-element sea ice/ice shelf/ocean model, Ann. Glaciol., 53, https://doi.org/10.3189/2012AoG60A156, 2012.

Urruty, B., Hill, E. A., Reese, R., Garbe, J., Gagliardini, O., Durand, G., Gillet-Chaulet, F., Gudmundsson, G. H., Winkelmann, R., Chekki, M., Chandler, D., and Langebroek, P. M.: The stability of present-day Antarctic grounding lines – Part A: No indication of marine ice sheet instability in the current geometry, The Cryosphere Discussions, 2022, 1–34, https://doi.org/10.5194/tc-2022-104, 2022.

Štulić, L., Timmermann, R., Paul, S., Zentek, R., Heinemann, G., and Kanzow, T.: Southern Weddell Sea surface freshwater flux modulated by icescape and atmospheric forcing, EGUsphere, 2023, 1–30, https://doi.org/10.5194/egusphere-2023-690, 2023.

Zweng, M. M., Reagan, J. R., Antonov, J. I., Locarnini, R. A., Mishonov, A. V., Boyer, T. P., Garcia, H. E., Baranova, O. K., Johnson, D. R., Seidov, D., and Biddle, M. M.: World Ocean Atlas 2013, Volume 2: Salinity, in: NOAA Atlas NESDIS 74, edited by Levitus, S. and Mishonov, A., p. 39 pp, 2013.